NeuroImage **9,** 195–207 (1999)
Article ID nimg.1998.0396, available online at http://www.idealibrary.com on IDEAL®

Cortical Surface-Based Analysis

II: Inflation, Flattening, and a Surface-Based Coordinate System

Bruce Fischl,* Martin I. Sereno,† and Anders M. Dale*,[1]

*Nuclear Magnetic Resonance Center, Massachusetts General Hosp/Harvard Medical School, Building 149, 13th Street, Charlestown, Massachusetts 02129; and †Department of Cognitive Science, University of California at San Diego, Mailcode 0515, 9500 Gilman Drive, La Jolla, California 92093-0515

Received May 27, 1998

The surface of the human cerebral cortex is a highly folded sheet with the majority of its surface area buried within folds. As such, it is a difficult domain for computational as well as visualization purposes. We have therefore designed a set of procedures for modifying the representation of the cortical surface to (i) inflate it so that activity buried inside sulci may be visualized, (ii) cut and flatten an entire hemisphere, and (iii) transform a hemisphere into a simple parameterizable surface such as a sphere for the purpose of establishing a surface-based coordinate system. © 1999 Academic Press

Key Words: **Cortical surface reconstruction, flattening, coordinate systems, atlas.**

1. INTRODUCTION

Currently, the most widely used method of analyzing functional brain imaging data is to project the functional data from a sequence of slices onto a standardized anatomical 3-D space. The most common of these procedures is based on the Talairach atlas (Talairach *et al.*, 1967; Talairach and Tournoux, 1988; see, e.g., Collins *et al.*, 1994, for an automated procedure). While this type of approach has certain advantages (ease of use, widespread acceptance, applicability to subcortical structures), it also has significant drawbacks.

These drawbacks derive from the fact that the intrinsic topology of the cerebral cortex is that of 2-D sheet with a highly folded and curved geometry. Estimates of the amount of "buried" cortex range from 60 to 70% (Zilles *et al.*, 1988; Van Essen and Drury, 1997), implying that distances measured in 3-D space between two points on the cortical surface will substantially underestimate the true distance along the cortical sheet, particularly in cases where the points lie on different banks of a sulcus.

From a functional standpoint, nonhuman primate neocortex is composed of a mosaic of visual, auditory, somatosensory, and motor areas, with visual areas alone occupying more than half of the total cortical surface area (Felleman and Van Essen, 1991; Kaas and Krubitzer, 1991; Sereno and Allman, 1991). The bulk of the remaining half is composed of auditory, somatosensory, motor, and limbic areas, each occupying about ⅛ of the total neocortex (Morel and Kaas, 1992; Stepniewska *et al.*, 1993).

The majority of these areas are defined by their topographic maps of the sensory periphery (e.g., retinotopic, tonotopic, somatotopic). Typically, the metric encoding the relationship between these maps and the sensory periphery which they represent is not known (see, Schwartz, 1977, 1980, for a notable exception). However, the two-dimensional nature of the maps as well as their topographic arrangement strongly suggest that a two-dimensional surface-based metric is more appropriate for analyzing their functional properties than the more typically used volume-based metrics.

The highly folded nature of the cortical surface also makes it difficult to view functional activity in a meaningful way. The typical means of visualization of this type of data is the projection of functional activation onto a set of orthogonal slices. This procedure is problematic as regions of activity which are close together in the volume may be relatively far apart in terms of the distance measured along the cortical surface. In addition, the naturally two-dimensional organization of cortical maps is largely obscured by the imposition of an external coordinate system in the form of orthogonal slices. These problems have led an increasing number of studies to make use of surface-based techniques for visualization (Tootell *et al.*, 1995; DeYoe *et al.*, 1996; Engel *et al.*, 1997; Reppas *et al.*, 1997; Talavage *et al.*, 1997; Van Essen and Drury, 1997; Hadjikhani *et al.*, 1998; Moore *et al.*, 1998).

[1] To whom correspondence and reprint requests should be addressed. Fax: (617) 726-7422. E-mail: dale@nmr.mgh.harvard.edu.

1053-8119/99 $30.00
Copyright © 1999 by Academic Press
All rights of reproduction in any form reserved.

In order to facilitate the use of surface-based techniques for both display and analysis of structural and functional properties of the cerebral cortex, we have developed a unified procedure which begins with a previously reconstructed cortex (Dale and Sereno, 1993; Dale *et al.*, 1998) and modifies it in order to achieve three separate but related goals:

(1) The "inflation" of the cortical surface so that activity occurring inside sulci may be easily visualized.

(2) The flattening of an entire hemisphere so that the activity across the hemisphere may be seen from a single view, and so that computational procedures which are not tractable on arbitrary manifolds may be employed in the analysis of the cerebral cortex.

(3) The "morphing" of a hemisphere into a surface, which maintains the topological structure[2] of the original surface, but has a natural (i.e., closed-form) coordinate system.

Using the methods described in this paper we have been able to map out the detailed topographic organization of human retinotopic visual areas (Sereno *et al.*, 1995; Tootell *et al.*, 1996a,b, 1997, 1998a,b), the tonotopic structure of primary auditory cortex (Talavage *et al.*, 1996, 1997a,b, 1998a,b), the topography of primary somatosensory cortex (Moore *et al.*, 1997, 1998; Moore, 1998), as well as areas involved in the processing of visual motion (Tootell *et al.*, 1995; Reppas *et al.*, 1997; Culham *et al.*, 1998), color (Hadjikhani *et al.*, 1998), perception of faces and objects (Halgren *et al.*, 1998), and processing the meaning of words (Halgren *et al.*, 1998). In addition, the cortical surface reconstruction has been used to constrain the EEG/MEG inverse problem (Dale and Sereno, 1993; Liu *et al.*, 1996; Liu *et al.*, 1998a,b). The cortical surface reconstruction, visualization, and analysis tools described here and in a companion article (Dale *et al.*, 1998) are based on the methods previously described by Dale and Sereno (1993).

2. MAPPING OF THE CORTICAL SURFACE TO PARAMETERIZABLE SHAPES

Because of the varying intrinsic curvature of the cortical surface it is not possible to map it onto other significantly smoother surfaces (such as planes or spheres) without introducing some metric and/or topological distortion into the surface representations (do Carmo, 1976). A mapping between two surfaces with no metric distortion is called an isometry. Finding such a mapping from the sphere to the plane has been called the mapmaker's problem and was shown to be impossible by Gauss (1828), as the surfaces in question have differing intrinsic (or Gaussian) curvature. Nevertheless, for representations to be useful for either visualization or computational purposes, metric distortion must be minimized. Toward that end, we have developed a general procedure for minimizing metric distortion in a variety of contexts, such as surface inflation, flattening, as well as mapping to other parameterizable surfaces such as a sphere.

Constructing this type of mapping is a difficult task due to the complex and highly folded nature of the original surface, which requires a fine-scale tessellation in order to capture its metric and topological properties. One attractive means of flattening the surface is the method employed by Schwartz and colleagues (Schwartz and Merker, 1986; Schwartz *et al.*, 1989; Wolfson and Schwartz, 1989), in which the matrix of distances of each vertex to all other vertices is constructed in order to represent the metric properties of the original surface. The surface is then randomly projected onto a plane and unfolded in such a way as to minimize the mean-squared error between the original distance matrix and that of the flattened surface. While this method is more than adequate for flattening small patches of the cortical surface, such as primary visual cortex to which it was originally applied, the computational requirements of the procedure in terms of both memory and time become prohibitive as the patch size grows.

A different type of method was employed by Dale and Sereno (1993), and later by Carman *et al.* (1995) as well as Drury and Van Essen (Drury *et al.*, 1996; Van Essen and Drury, 1997; Van Essen *et al.*, 1998). In this approach, a variety of local forces are constructed in order to encourage the preservation of local area and conformality (i.e., angle), while also forcing the surface to unfold onto a plane. These techniques have been successfully applied to entire cortical hemispheres, but suffer from a number of drawbacks. First, they require the use of terms such as a spring force in order to eliminate folds, which results in surfaces that are not optimal with respect to the preservation of any metric property. In addition, they treat the vertices on the borders of the flattened surface differently than those in the interior, thus constraining the shape of the resulting surface. Finally, they preserve only local properties of the surface and therefore do not rule out large-scale distortions caused by locally correlated errors, although the use of multiresolution techniques addresses this concern to some degree.

Part of the problem with applying the Schwartz method is that relatively long-range distances must be accounted for in order to unfold patches of cortex which have been folded by the projection process. They estimate that a procedure incorporating distance con-

[2] The term topological structure is frequently used to refer to the border of a domain as opposed to its global topology (Mortenson, 1997). For example, once an incision has been made in the cortical surface it is topologically equivalent to a plane. Further incisions alter its topological structure, but not its topology (unless they result in multiple disconnected components).

straints on the order of 1 cm suffices to unfold monkey V1 (Schwartz *et al.*, 1989). Unfortunately, the distance required to smooth out a fold grows with the size of the surface (and the fold), quickly requiring untenable memory usage. Using a random subsampling of the distance matrix alleviates this problem to some extent, but not to the degree required to flatten an entire cortical hemisphere.

This problem occurs because distances are unoriented, and therefore mirror image configurations represent local minima in the energy functional. To see this, imagine a piece of paper folded exactly along a string of vertices. If only nearest neighbor distances are being preserved, this represents an optimal configuration with the same energy as the completely unfolded state. The inclusion of neighborhoods which are small relative to the size of the entire sheet will not aid the problem, as the majority of the nodes on the surface are then beyond the neighborhood of the fold. This type of situation thus represents a local minimum, as moving vertices along the fold will increase the metric error until the rest of the surface expands. In order to cause the surface to unfold, a sufficient number of vertices must be included in the distance matrix so that the decrease in error caused by removing the fold more than offsets the increase in error of the region outside the fold, a solution that is not viable for as complex and large a surface as an entire cortical hemisphere.

We therefore construct a means of encouraging the surface to unfold which satisfies three criteria: (1) The final surface should be optimal with respect to minimizing metric distortion. (2) The borders of the cut surface should be treated no differently than the interior. (3) The resulting surface should have only minimal folding.

The first two criteria exclude the use of spring terms to "regularize" the mesh, which are typically introduced in order to prevent folding. Instead, we construct an energy functional that employs only a distance term for unfolded or positive regions of the surface, but applies an additional term to folded or negative regions in order to cause the surface to unfold. This term makes use of the embedding space to give the normal vector field of the surface a consistent orientation (positive z in the plane, radially outward on the sphere). Any triangles in the tessellation for which the ordered cross-product of its legs is antiparallel to the normal direction is then assigned a negative area.[3] Constraining the area to be positive everywhere eliminates folds in the surface.

The spherical and flattening transformations thus proceed as follows. First, geodesic distances are estimated on the original (folded) surface, after the introduction of cuts in the flattened case. Note that after the surface has been cut, only the remaining vertices are considered in the distance calculations. Next, the cortical manifold is projected onto the target surface and assigned a normal vector field with a consistent orientation (the inflation procedure does not require a projection step as the energy functional used in the inflation process contains a term which drives the surface toward the target configuration). The potentially large folds and metric distortions introduced by the projection process are then removed by minimizing an energy functional, which contains terms representing these two factors separately. The resulting surfaces have essentially no remaining folds and only minimal metric distortion.

2.1. Minimizing Metric Distortions

The term that minimizes metric distortions is constructed as follows. Consider a mesh of V vertices distributed irregularly over a surface S embedded in a 3-D Cartesian space. Denoting the distance between the ith and jth vertices at iteration number t of the numerical optimization procedure by d_{ij}^t, we construct a mean-squared energy functional J_d:

$$J_d = \frac{1}{4V}\sum_{i=1}^{V}\sum_{n\in N(i)}(d_{in}^t - d_{in}^0)^2,\ d_{in}^t = \|\mathbf{x}_i^t - \mathbf{x}_n^t\| \quad (1)$$

where $\mathbf{x}_i^t$ is the (x, y, z) position of vertex i at iteration number t, d_{in}^0 is the distance between the i^{th} and n^{th} vertices on the original cortical surface before projection, and $N(i)$ is the set of vertices defined to be in the neighborhood of vertex i.[4] Taking the partial derivative of J_d with respect to the k^{th} vertex results in

$$\frac{\partial J_d}{\partial \mathbf{x}_k} = \frac{1}{V}\sum_{n\in N(k)}(d_{kn}^t - d_{kn}^0)\mathbf{e}_{kn}, \quad (2)$$

where $\mathbf{e}_{kn}$ is a unit vector pointing from vertex k to vertex n. This term is similar to the "longitudinal" one employed by Carman *et al.* (1995), except here it is identified as the gradient of a well-defined energy function, and the distances we employ are along significant sections of the manifold, as opposed to simply representing the spacing of the mesh.

2.2. Long Range-Distance Calculation

The problem of computing geodesic distances on an arbitrary manifold is a difficult one. One solution is to

[3] This oriented area term can be seen as the determinant of the Jacobian matrix of the transformation.

[4] The $\frac{1}{4}$ scaling factor removes the factor of 2 introduced by taking the derivative of the quadratic distance term as well as an additional factor of 2 that accounts for all the symmetric terms in which $\mathbf{x}_k$ appears as a neighbor of another vertex.

use the faces of the polyhedral approximation to compute the exact geodesic distances, as suggested by Wolfson and Schwartz (1989). Unfortunately, the time requirements of this algorithm are exponential in the number of triangles in the tessellation, which makes it computationally untenable if millimeter resolution is desired for the surface. While decimation techniques may be employed to reduce the size of the surface representation, it is not clear that the reduction would be sufficient to make the use of this algorithm feasible, as on the order of 300,000 triangles are required to cover a typical human cortex and single millimeter-sized structures are common.

A simpler technique that is computationally tractable is to take a dynamic programming approach to the calculation of distances and employ an algorithm typically used to calculate minimal distances in a graph (Dijkstra, 1959). Here we modify it slightly, as the graph in question is the tessellation of the cortical surface. This requires a minor correction in the form of a scaling factor, so that the distance estimates on the cortical manifold are essentially unbiased with respect to the geodesic distances.

The Dijkstra algorithm for computing distances proceeds as follows. For each vertex we label each of its nearest neighbors as 1-neighbor and compute the Euclidean distance from them to the central vertex. We then label each neighbor of a 1-neighbor that is not already labeled (and is not the central vertex) as a 2-neighbor. Next, we examine the neighbors of each 2-neighbor and find the one with the shortest distance to the central vertex. We then compute the distance to the 2-neighbor as the distance of the optimal neighbor plus the length of the edge connecting them. This procedure is then applied iteratively with the neighborhood size expanding at each iteration. One point to note is that the resulting distances are similar to a Manhattan metric in that they typically overestimate the geodesic distance. In order to alleviate this problem we scale the resulting distances by ((1 + sqrt(2))/2). This correction factor results in an estimate which is essentially zero mean,[5] with the variation from the true distance acting as white noise, a factor we will show is negligible in section 6.

2.3. Unfolding Using Oriented Area

As noted previously, causing the surface to unfold using only a distance term is not feasible for large surfaces. This is due to the fact that mirror-image configurations are not directly penalized, resulting in folded states that are local minima of the energy functional. These local minima are caused by the inherently unoriented nature of distances that do not explicitly distinguish between folded and unfolded states. In order to resolve this problem, we therefore seek an oriented metric property that discourages folds in the surface. The two obvious candidates are conformality and areal terms. While both can be employed successfully in this context, the use of an angle term results in a gradient that is dependent on the square of the inverse of the vertex spacing and is therefore somewhat numerically unstable. In contrast, the use of an oriented area results in a quadratic energy functional.

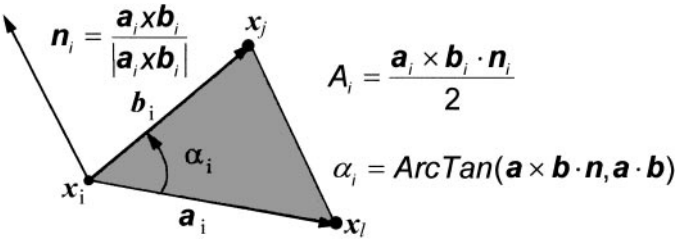

FIG. 1. Metric properties of the triangular tessellation.

In order to define the areal term of the energy functional we consider the ith triangle in the surface tessellation depicted in Fig. 1, with unit normal vector $\mathbf{n}_i$ and edges $\mathbf{a}_i$ and $\mathbf{b}_i$ connecting the vertex x_i to two of its neighbors (note that bold-faced symbols denote vector quantities). The unit normal $\mathbf{n}_i$ is given on the original manifold by the normalized cross product of the edges $\mathbf{a}_i$ and $\mathbf{b}_i$, while the area of the triangle is half the cross product of $\mathbf{a}_i$ and $\mathbf{b}_i$ dotted with the unit normal (i.e., the triple scalar product). However, for other representations such as spherical and flattened, the normal vector field can be given a consistent orientation on the surface[6] using the embedding space, and A_i becomes an oriented area, which may take on negative values, indicating folds in the surface.

Given this description of the metric properties of the surface through the triangular tessellation, we form an energy functional J_a that penalizes negative area in proportion to the difference between the current area and the original area occupied by each triangle:

$$J_a = \frac{1}{2T}\sum_{i=1}^{T} P(A_i^t)(A_i^t - A_i^0)^2,\ P(A_i^t) = \begin{cases} 1, & A_i^t \le 0 \\ 0, & otherwise, \end{cases} \qquad (3)$$

where, as before, superscripts denote time, with 0 being the areal values on the original cortical surface, T refers to the number of triangles in the tessellation, and the functional dependence of the A_is on the position of

[5] The scaling factor we use is representative of the rectangular nature of the tessellation, as it is constructed directly from voxel faces. A different scaling factor is required for other tessellation techniques.

[6] This is always possible except in pathological cases such as the Möbius strip which are said to be *nonorientable* (do Carmo 1976).

the vertex and its neighbors has been suppressed for simplicity of notation. This term ensures that the transformation is one-to-one and therefore has a well-defined inverse, by preventing folds in the surface which would represent the mapping of multiple points to the same location in the embedding coordinate system.

In order to minimize J_a, we take the gradient with respect to the vertex positions $\mathbf{x}_k$:

$$\frac{\partial J_a}{\partial \mathbf{x}_k} = \frac{1}{T}\sum_{i=1}^{T}(A_i^t - A_i^0)\frac{\partial A_i^t}{\partial \mathbf{x}_k}. \tag{4}$$

Expanding the partial derivative using the chain rule yields:

$$\frac{\partial A_i^t}{\partial \mathbf{x}_k} = \frac{\partial A_i^t \partial \mathbf{a}_i}{\partial \mathbf{a}_i \partial \mathbf{x}_k} + \frac{\partial A_i^t \partial \mathbf{b}_i}{\partial \mathbf{b}_i \partial \mathbf{x}_k}, \frac{\partial A_i^t}{\partial \mathbf{a}_i} = \mathbf{b}_i \times \mathbf{n}_i \frac{\partial A_i^t}{\partial \mathbf{b}_i} = \mathbf{n}_i \times \mathbf{a}_i. \tag{5}$$

The partials of the change in the legs with respect to a change in the vertex position are dependent on what position the vertex in question occupies in a given triangle:

$$\frac{\partial a_i}{\partial \mathbf{x}_k} = \begin{cases} [-1,-1,-1]^T, & k = i \\ [1,1,1], & k = l \\ 0, & otherwise \end{cases}, \quad \frac{\partial \mathbf{b}_i}{\partial \mathbf{x}_k} = \begin{cases} [-1,-1,-1]^T, & k = i \\ [1,1,1], & k = j \\ 0, & otherwise, \end{cases} \tag{6}$$

2.4. The Complete Energy Functional

The complete energy functional incorporating both distance and areal terms is given by

$$J = \lambda_d J_d + \lambda_a J_a, \tag{7}$$

where the λ_a and λ_d coefficients define the relative importance of unfolding versus the minimization of metric distortions respectively. Initially, λ_a takes on values much larger than λ_d, and gradually decreases over time as the surface successfully unfolds. One additional point to note is that we smooth the gradients using iterative averaging during the numerical integration. This allows entire regions that are compressed or expanded to move coherently in the appropriate direction, and is similar to decimation followed by upsampling with interpolation. We allow each scale (defined by the number of iterations in the averaging) to equilibrate before reducing the scale and continuing. The actual minimization of $J(\mathbf{x})$ is accomplished using gradient descent with line minimization (Press *et al.*, 1994), as detailed in the appendix.

3. SURFACE INFLATION

The high degree of folding of the cortical surface makes it desirable to inflate the reconstructed surface for visualization purposes (Dale and Sereno, 1993). This renders the interior of sulci visible, as well as making the surface-based distance between regions more apparent to visual inspection. The purpose of the surface inflation is thus to provide a representation of the cortical hemisphere that retains much of the shape and metric properties of the original surface, but allows the visualization of functional activity occurring within sulci. For this purpose, we define an energy functional, the minimization of which results in the desired shape. This functional consists of two terms, a spring force which smooths the surface, and the metric-preservation term described in Section 2.1, which constrains the evolving surface to retain as much of the original metric properties as possible:

$$J_s = \frac{1}{2V}\left(\sum_{i=1}^{V}\sum_{n\in N_1(i)}\|\mathbf{x}_i - \mathbf{x}_n\|^2\right) + \lambda_d J_d, \tag{8}$$

where N_l denotes the set of nearest neighbors of each vertex, J_d is as defined in Section 2.1, and a value of 0.1 for the coefficient λ_d yields smooth surfaces with minimal metric distortion. Larger values of λ_d result in reduced metric distortion at the cost of generating less smooth surfaces.

We use Euler's method with momentum to integrate J_s until the surface has achieved a desired smoothness as measured by the goodness-of-fit of the polyhedral approximation.[7] Note that, in contrast to the flattening and spherical transformation, the surface inflation does not require a projection step, as the spring term serves to drive the surface toward the desired smoother configuration.

One further point to note is that the inflation process is driven by the average convexity or concavity of a region. That is, points which lie in concave regions move outwards over time, while points in convex regions move inwards. Thus, integrating the normal movement of a point during inflation provides a measure of average convexity or concavity at that point. Formally, the average convexity $C(\mathbf{x}_k^0)$ at position $\mathbf{x_k}$ on the original surface is given by:

$$C(\mathbf{x}_k^0) = \int \left(\frac{\partial J_s}{\partial \mathbf{x}_k^t} \cdot \mathbf{n}(k)\right) dt, \tag{9}$$

where $\mathbf{n}(k)$ is the unit normal vector to the surface at the k^{th} vertex in the tessellation at time t. Vertices that consistently move outwards, or parallel to the normal direction, will have a large positive value of C, while

[7] We integrate the inflation functional until the normalized average distance of the neighbors of each vertex from its tangent plane is below a prespecified threshold.

points that move antiparallel to the normal will be assigned large negative values.

The average convexity is useful for quantifying the folding pattern of a surface, as C captures large-scale geometric features, while being relatively insensitive to the small folds that typically occur on the banks of a sulcus. This is in contrast to mean curvature which attains equally high values for small secondary and tertiary folds in a surface as for the primary folds. Figure 3 illustrates this difference between the mean curvature of the folded cortex (left) and the average convexity as quantified by C (right), painted onto both the gray/white matter (top), and inflated (bottom) surfaces. Note how accurately the average convexity represents only the primary folding patterns. The major anatomical features of this surface, such as the central sulcus (CS), superior temporal sulcus (STS), intraparietal sulcus (IPS), and sylvian fissure (SF), are clearly visible, while the secondary and tertiary folding patterns apparent in the mean curvature are largely absent. In our standard analysis procedure we use C as a means for quantifying the folding pattern of a surface as it is insensitive to noise in the form of small wrinkles in a surface and relatively stable across individuals (see Fischl *et al.*, 1998).

4. FLATTENING

In order to flatten a cortical hemisphere with minimal distortion we make a number of cuts on the medial aspect of the original surface—one in a region around the corpus callosum to remove all midbrain structures, one down the fundus of the calcarine sulcus, a set of equally spaced radial cuts, as well as a sagittally oriented cut around the temporal pole (see Fig. 4). This pattern of cuts removes most of the intrinsic curvature of the surface, allowing it to be flattened with only minor distortion, while preserving the topological structure of the lateral aspect of the surface. Several alternative cutting schemes have been suggested by others (DeYoe *et al.*, 1996; Drury *et al.*, 1996). The optimal choice of cuts depends on which parts of the surface one is most interested in preserving for a particular application. For example, in our standard analysis of visual data, we make a planar cut that detaches the posterior part of the brain including all of the occipital lobe, and parts of the parietal and temporal lobes. We then introduce a cut down the fundus of the calcarine sulcus, which separates the upper and lower visual fields of the retinotopic areas and removes most of the intrinsic curvature of the remaining surface. Currently, the surface cuts are made manually by a trained operator, based on anatomical landmarks. In the future, it should be possible to automate the cutting process, by specifying the coordinates of the cuts in a surface-based coordinate system (Fischl *et al.*, 1998; Thompson *et al.*, 1998; Sereno *et al.*, 1996; Van Essen *et al.*, 1997).

Once the desired cuts have been made, we project the resulting surface onto a plane whose normal is given by the average surface normal of the cut surface (that is, the portion of the original surface which remains after the cutting process). After the projection has been accomplished, we give the flattened surface a consistent orientation by setting the normal vector field to $[0,0,1]^T$ and allow the surface to unfold by minimizing the energy given in Section 2.4, using angularly spaced randomly sampled distances in a 0.8 cm radius of each vertex as the neighborhood $N(i)$.[8] The result of this procedure is shown in Fig. 5, which depicts three flattened left hemispheres.

5. SPHERICAL TRANSFORMATIONS AND A SURFACE-BASED COORDINATE SYSTEM

Identifying corresponding points on different cortical surfaces requires the establishment of a uniform surface-based coordinate system (Drury *et al.*, 1996; Sereno *et al.*, 1996; Thompson *et al.*, 1996; Thompson and Toga, 1996; Davatzikos, 1997; Van Essen and Drury, 1997; Fischl *et al.*, 1998). This is in contrast to volume-based coordinate systems in which a point on the cortical surface in one volume will typically not lie on the cortical surface of a different volume. In order to establish a surface-based coordinate system, we transform the reconstructed cortical surface into a parameterizable surface, as the parameterization then provides a natural coordinate system. The surface we choose for this purpose is a sphere for a number of reasons. This choice is primarily motivated by the fact that the mapping of the cortical hemisphere onto a sphere allows the preservation of the topological structure of the original surface (i.e., the local connectivity). This is in contrast to the use of a flattened surface, which requires cuts to be introduced prior to flattening in order to minimize distortion. These cuts change the topological structure of the surface, resulting in points on opposite sides of a cut, which are close to each other on the original cortical surface, becoming quite far apart in the final flattened representation. The choice of the sphere also allows us to retain much of the computational attractiveness of a flat space, facilitating the calculation of metric properties such as geodesic distances, areas, and angles, properties that are more difficult to compute on less symmetric surfaces such as ellipsoids.

[8] At each distance we enforce a minimal angular spacing between the sampled points. This spacing is based on the number of neighbors selected at each extent. For the flattening we sample 8 points at each distance out to 8 cm, forcing the points to be separated by as close to $2\pi/8$ radians as possible.

The process of unfolding the cortical surface on a sphere is identical to the flattening procedure outlined in Section 4, except that distances on the sphere are no longer Euclidean, but rather must be computed using the geodesics of the sphere. In the spherical case, we give the surface a consistent orientation by using an outwards pointing normal vector field:

$$\mathbf{n_i} = \frac{\mathbf{x_i}}{\|\mathbf{x_i}\|} \tag{10}$$

where $\mathbf{x}_i$ refers to the vector from the center of the sphere to the i^{th} vertex. In addition, the lack of freedom to modify the shape of the unfolding surface necessitates the use of longer range distances than in the case of the flattening. In order to generate the spherical representation, we first project the inflated cortical surface onto the unit sphere by moving each vertex in the tessellation of the inflated surface to the closest point on the sphere. Next, we allow the surface to unfold by minimizing the metric distortions introduced by the inflation and projection procedures. These distortions are estimated based on an angularly spaced random sampling of distances in a 1-cm radius of each vertex. The surface is projected back onto the sphere at each step in the minimization procedure. Figure 6 illustrates the result of applying this procedure to three cortical hemispheres.

Once the spherical representation has been established, we can use any of the standard spherical coordinates systems (e.g., longitude and colatitude) to index a point on any of the surface representations for a given subject (Fig. 7). Furthermore, in other work (Sereno *et al.*, 1996; Fischl *et al.*, 1998), we have developed a procedure for aligning cortical hemispheres with an average surface, based on the average convexity measure C defined by Eq. (9). By maximizing the correlation of the convexity measure between the individual and the average, the procedure computes an optimal mapping to a "canonical" surface and hence a surface-based coordinate system. This type of surface-based approach, which a number of groups are working on (Drury *et al.*, 1996, 1997; Thompson *et al.*, 1996; Thompson and Toga, 1996; Davatzikos, 1997), can increase the accuracy of localizing anatomically consistent functional areas by a factor of three over volume-based techniques (Fischl *et al.*, 1998), as well as providing a means for high-resolution intersubject averaging of functional data occurring on the cortical surface.

6. ERROR ANALYSIS

There are a number of concerns which must be addressed in regard to using the corrected Dijkstra algorithm as an estimator of geodesic distances. The most important of these concerns the accuracy of the metric properties of surfaces flattened using these distances. Another consideration is to what degree these surfaces diverge from surfaces flattened using true geodesic distances as targets. A third question is in regard to the accuracy of the flattening procedure applied to surfaces which contain varying amounts of intrinsic curvature.

In order to assess these issues, we flattened a set of surfaces for which analytic geodesic distance expressions exist, namely a plane and various portions of a sphere. The entire set of surfaces were flattened twice, once using the corrected Dijkstra distances as targets, and once with the targets computed using the true geodesic distances. The results of this analysis are depicted in Fig. 8. The x-axis in this plot is a measure of the curvature of the original surfaces, beginning with a plane at the far left ($x = 0$), and proceeding to increasing portions of a sphere, with a full hemisphere at the far right ($x = 50\%$). The y-axis represents the percentage distance error of the flattened surfaces, measured using analytic expressions for geodesics on the original surfaces (great circles on the sphere and Cartesian distances in the plane). The solid line in this figure is a plot of distance error versus curvature for the surfaces flattened using the corrected Dijkstra distances, while the dotted line depicts the distance error for the same surfaces flattened using the actual geodesic distances as targets. As can be seen, the difference between the two is small (the maximum difference is 1.37%), indicating the overall accuracy of the flattening procedure. Furthermore, the convergence of the plots indicates the insensitivity of the corrected Dijkstra distances, as well as the flattening procedure in general, to increasing curvature. The difference in percentage distance error for the two flattened hemispheres is less than 0.35%, suggesting that the error is dominated by the unavoidable distortions introduced by flattening a curved surface, rather than inaccuracies resulting from the use of the corrected Dijkstra distances as targets.

Finally, we present the errors of the flattening and spherical transformation on a set of 10 human hemispheres. All percentages in this section are computed using an L1 norm as it is less sensitive to outliers than the L2 norm. The transformation of the cortex into a sphere results in the largest metric distortion ($19.4 \pm 0.67\%$), presumably due to the lack of freedom to manipulate the borders on the closed shape. The flattening of the entire hemisphere gives rise to significantly smaller distortion ($11.7 \pm 0.42\%$), while the flattening of the posterior third of cortex, useful for analyzing visual areas, results in the smallest average distortion ($9.6 \pm 0.65\%$). The spatial distribution of metric distortions introduced by the flattening and spherical transformations are shown in Figs. 9 and 10, respectively, together with a histogram of the distortions in Fig. 11. The regions of high distortion for the

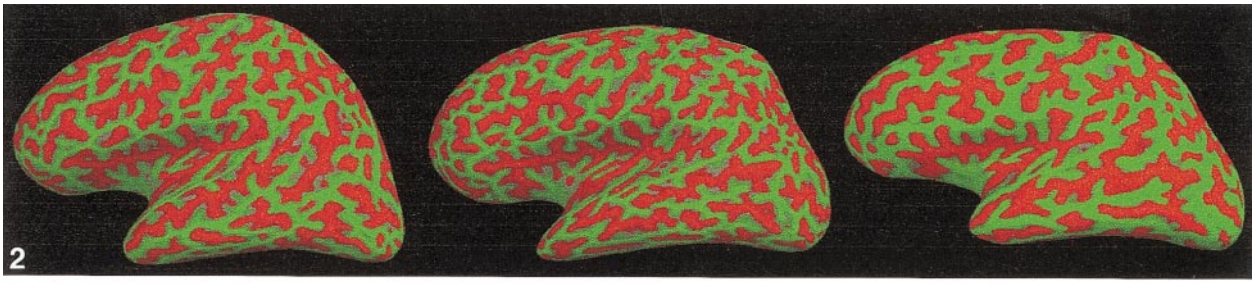

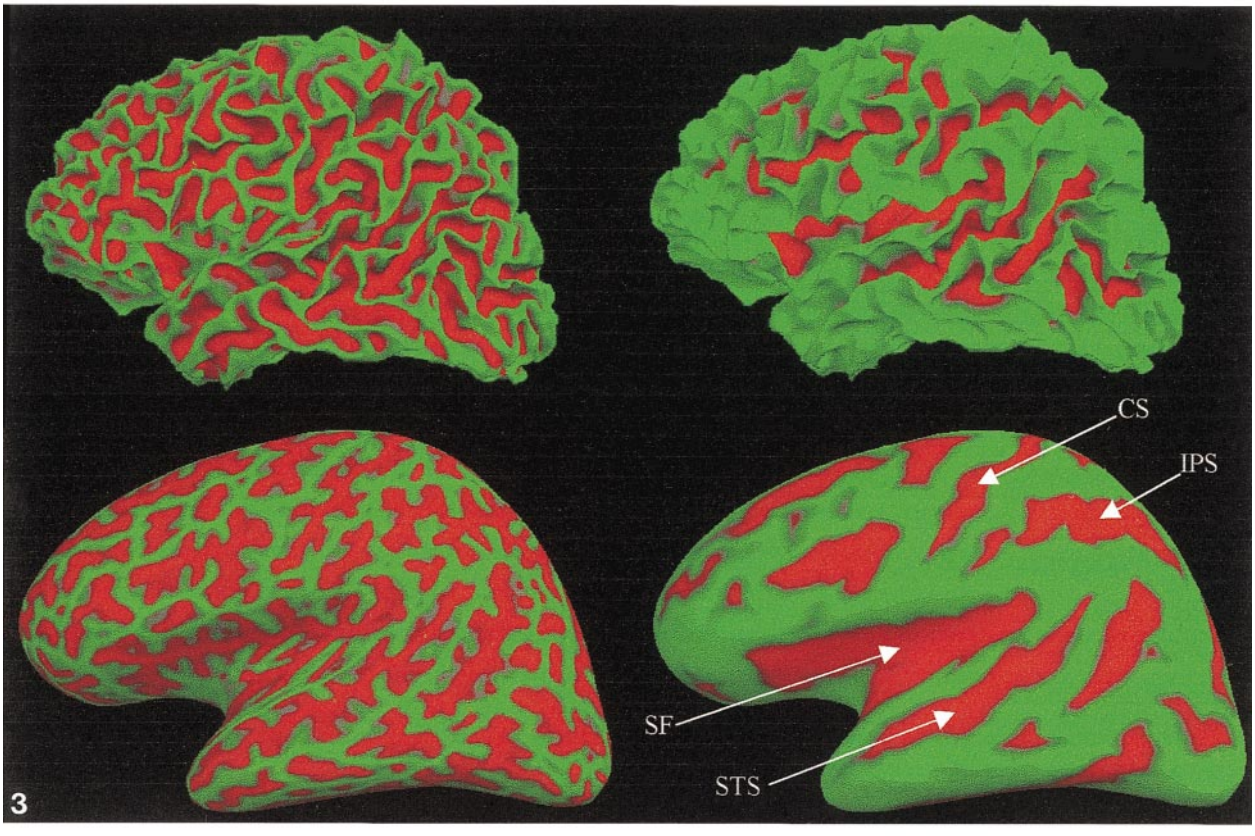

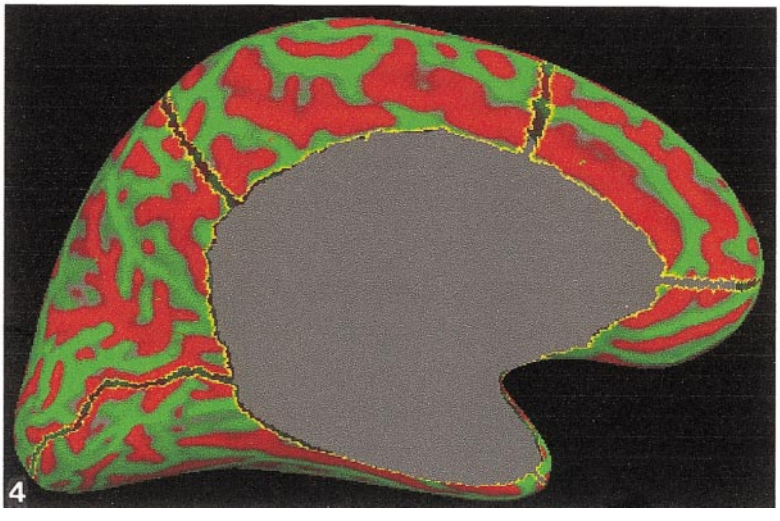

FIG. 2. Inflated representations of the three cortical surfaces (sulci are red and green are light).
FIG. 3. Mean curvature (left) and average convexity (right) painted onto folded (top) and inflated (bottom) representations of an individual subject's cortical surface.
FIG. 4. Medial view of an inflated surface after the introduction of cuts. Yellow regions indicate the borders of the cut surface.

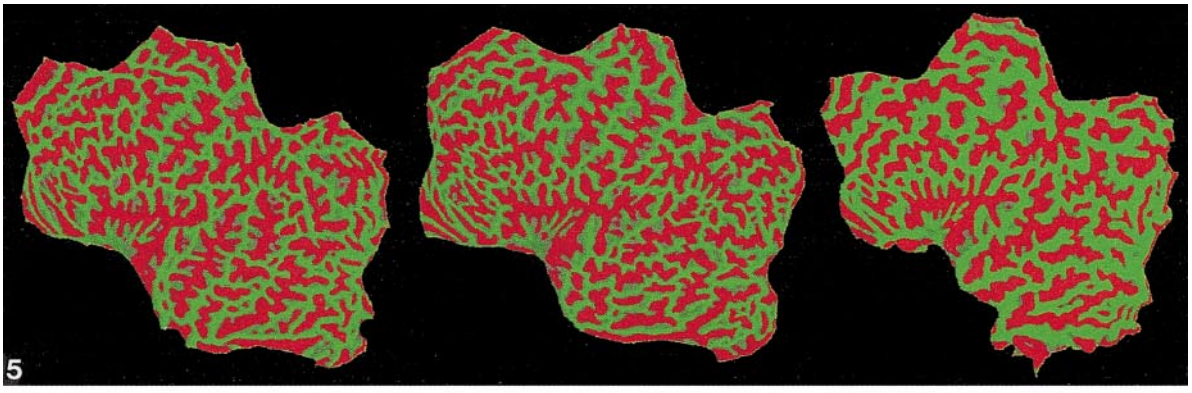

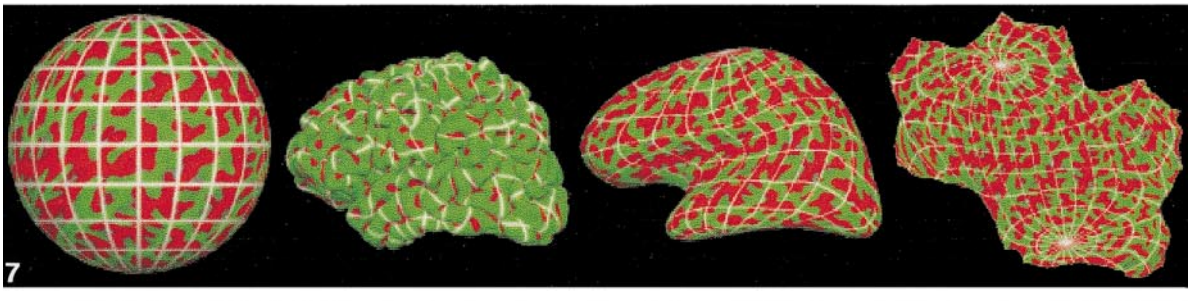

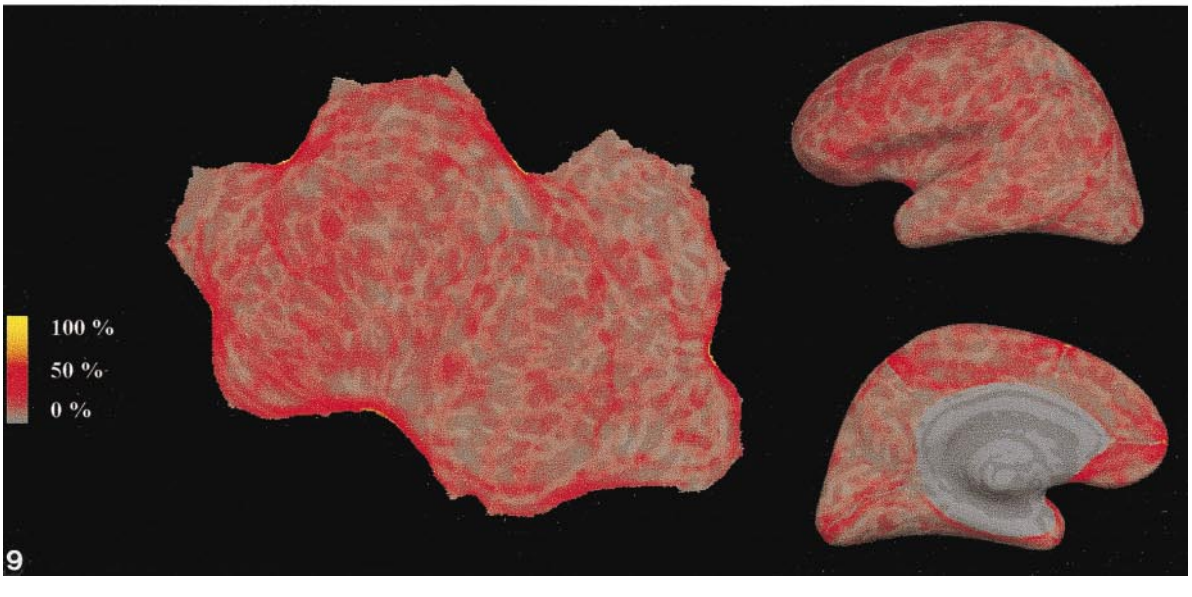

FIG. 5. Three flattened left hemispheres (sulci are red and green are light).
FIG. 6. Lateral view of three left hemispheres after spherical transformation.
FIG. 7. Spherical coordinate system painted onto a variety of surface representations.
FIG. 9. Spatial distribution of metric distortion introduced by the flattening, painted onto flattened (left), and inflated (right) representations (top—lateral view, bottom—medial view).

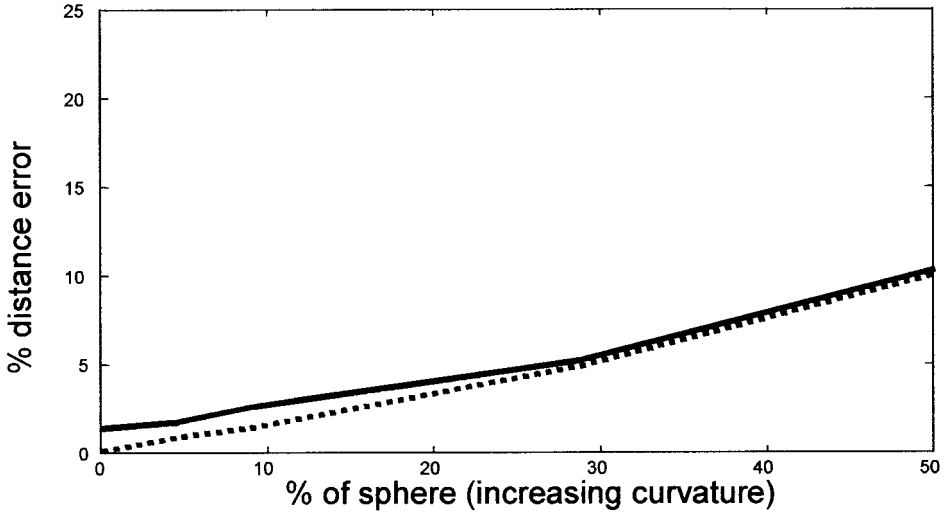

FIG. 8. Percentage distance error as a function of increasing curvature for surfaces flattened using corrected Dijkstra distances (solid) and true geodesic distances (dashed).

flattening are largely confined to the borders of the cut surface, with the interior having a relatively uniform small degree of distortion. The spherical transformation results in higher distortion, but this too is mainly confined to noncortical regions such as the lateral ventricle and the basal ganglia, where the surface is somewhat arbitrary. Thus, the actual mean error for cortical regions is probably a few percent lower than the numbers cited above, as evidenced by the mode of the two histograms in Fig. 11.

7. CONCLUSION

In this paper we have presented a unified set of procedures for transforming a previously reconstructed cortical surface. These transformations achieve two primary goals. First, they facilitate visualization of cortical activation patterns, including the detailed topographic organization of cortical areas, as well as distributed activity occurring across an entire hemisphere. In addition, such transformations enable two-dimensional

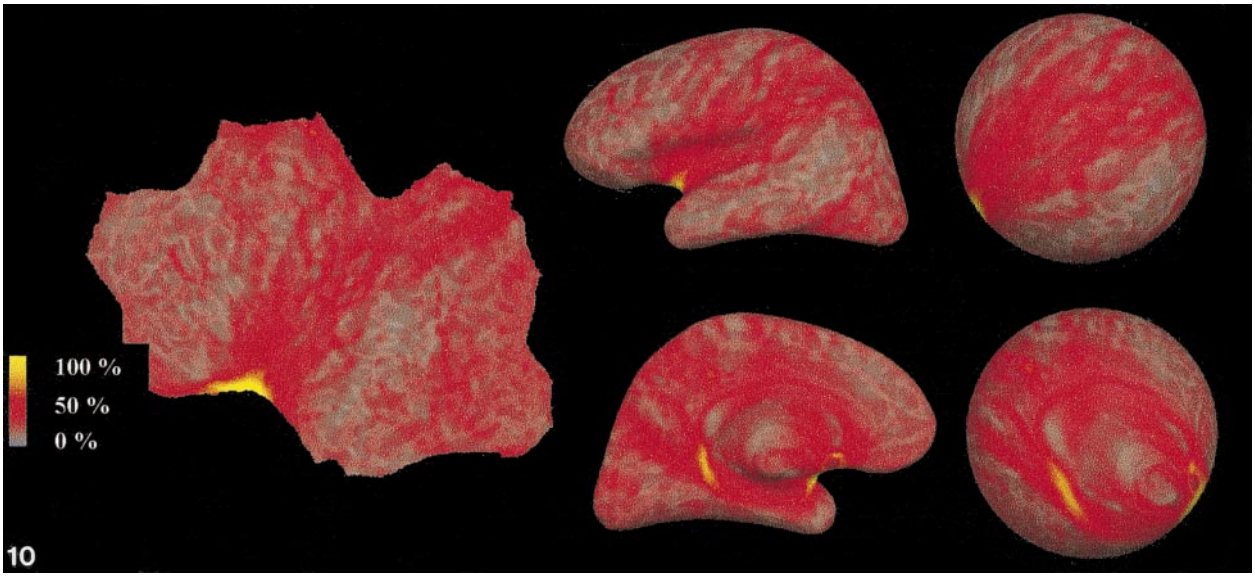

FIG. 10. Spatial distribution of metric distortion introduced by the spherical transformation, painted onto flattened (left), inflated (center), and spherical (right) representations of the same surface. Lateral and medial views are shown in the top and bottom rows, respectively.

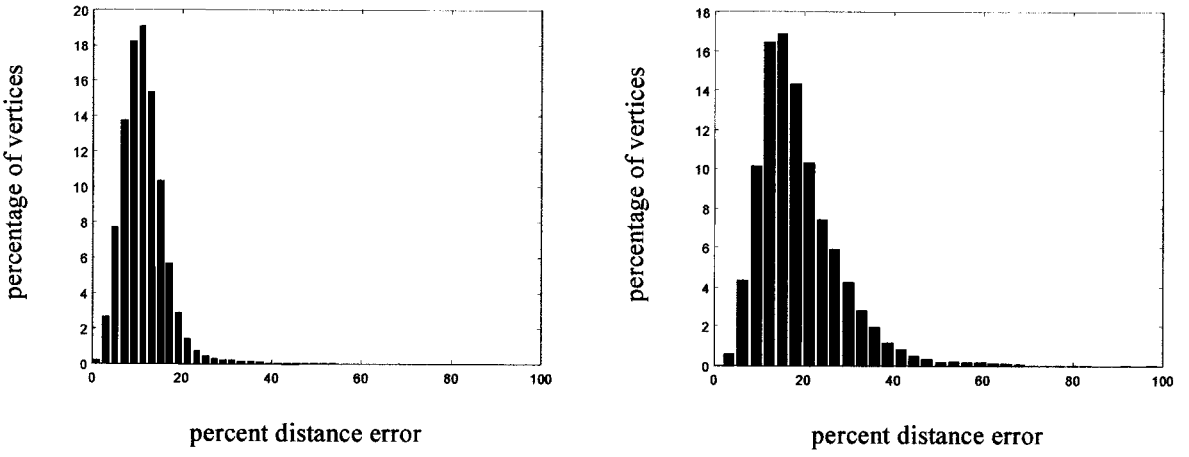

FIG. 11. Histogram of distance errors for the flattening (left) and spherical transformation (right) of a typical surface.

analysis techniques to be applied to the functional and structural properties of the cortical surface. The mapping procedures we have presented have the advantage of being optimal with respect to a well-defined energy functional that measures the amount of metric distortion and degree of folding of the transformed surface. In conjunction with segmentation methods, as described in the companion paper, these procedures allow the routine use of surface-based visualization and analysis of functional and structural properties of the human cortex.

8. APPENDIX

8.1. Numerical Integration

The numerical integration scheme we use is a form of multiscale line minimization that allows the surface to unfold robustly. Given an error functional $J^t(x)$ at time t, and its gradient ∇J with respect to the vertex positions, we will find the time step k which minimizes:

$$J^{t+1}(x) = J^t(\mathbf{x} + k\nabla J). \tag{11}$$

Since the surfaces typically have large folds due to the initial projection, simply setting k to a small value and performing gradient descent can be very costly. Instead, we search for the optimal k in a multiscale manner which permits macroscopic changes in the surface at each time step. Specifically, we first constrain k to be in the range $[k_{\min}, k_{\max}]$, where $k_{\min}$ and $k_{\max}$ are given by the smallest (0.1 mm) and largest (20 cm) allowable vertex movements, respectively, divided by the mean gradient magnitude. We then find the constant $k_1 = k_{\min}\, 10^l$ ($l = 0,1,2,\ldots$) which minimizes:

$$J^{t+1}(x) = J^t(\mathbf{x} + k_{\min}10^l\nabla J), \tag{12}$$

with the search terminating when $k_{\min}\, 10^l$ exceeds $k_{\max}$. That is, we sample $J^t(x + k\nabla J)$ in the range $[k_{\min}, k_{\max}]$ at order of magnitude intervals. Once we have determined k_1, and hence the proper scale to be searching for the optimal k, we then sample $J^t(x + k\nabla J)$ around k_1 at $k_2 = 1.5{*}k_1$ and $k_3 = 0.5{*}k_1$. Next, we fit a quadratic to these three values and compute the time step k_4, which would be optimal if the error surface were locally quadratic, as is frequently the case. Finally, we choose the time step k from the set $[0\ k_1\ k_2\ k_3\ k_4]$, which produces the smallest value of $J^t(x + k\nabla J)$, thus ensuring that $J(x)$ is monotonically decreasing with time.

8.2. Integration Schedule

As noted above, the surfaces frequently start with large folds due to the projection process. Unfolding the surface in this state usually requires that the areal term be large relative to the metric term in the energy functional $J(x)$ (that is, $\lambda_a \gg \lambda_d$). Conversely, after the surface has unfolded we will minimize the metric distortions and have the areal term be small. Thus, in the numerical integration we set the ratio λ_a/λ_d to be initially large, and let it decrease as the integration proceeds.

Another factor to consider is that the distortion introduced by the projection usually results in a gradient which is not locally coherent. This prevents the numerical integration scheme outlined above from finding large times steps which would unfold the surface in few iterations. One means of alleviating this problem would be to first unfold a decimated surface then interpolate to the full resolution and continue unfolding (Drury *et al.*, 1996). In this approach the decimation must be done in a manner which respects the local geometry of the surface. Instead, we take a simpler approach, and use a smoothed version of the gradient in the numerical integration, with the degree

of smoothing decreasing as the integration proceeds. The smoothing of the gradient has an effect similar to that of decimation: large regions of the surface move coherently. Since the surface has no well-defined metric, we are forced to use iterative averaging to perform the smoothing, a time consuming process.

Thus, the integration proceeds in epochs, where each epoch has a fixed λ_a/λ_d ratio. Typically we let λ_a/λ_d start at 1000 and decrease by factors of 10 until the surface has converged, with 5 epochs usually being sufficient to generate a near-optimal surface. We then set λ_a/λ_d large for one last epoch in order to smooth out any remaining folds in the surface (usually less than 0.05% of the surface is folded at this point). Within each epoch, we let the integration proceed using a fixed amount of gradient smoothing, until the decrease in the error functional asymptotes. After the error has asymptoted, we reduce the amount of smoothing and continue with the integration until the integration with the unsmoothed gradient has asymptoted, which signals the end of an epoch.

All the surfaces shown in this paper were generated in this manner, with each epoch beginning with 1024 iterations of gradient smoothing, and the amount of smoothing decreasing by factors of 4 until the integration using the unsmoothed gradient asymptoted. This procedure typically requires on the order of 15 h to flatten a full cortical hemisphere on a 266 MHz Pentium II, although slightly suboptimal surfaces can be obtained in about half that time.

ACKNOWLEDGMENTS

We are indebted to Eric Schwartz for many useful discussions about flattening. Thanks also go to Kevin Hall for testing and retesting the surface transformation routines, as well as to Arthur Liu for his numerous suggestions. And finally, we express our gratitude to one of the anonymous reviewers for many suggestions that helped make this a better paper.

REFERENCES

Atkins, M. S., and Mackiewich, B. T. 1996. *Automated Segmentation of the Brain in MRI.* The 4th International Conference no Visualization in Biomedical Computing, Hamburg, Germany.

Bullmore, E., Brammer, M., Rouleau, G., Everitt, B., Simmons, A., Sharma, T., Frangou, S., Murray, R., and Dunn, G. 1995. Computerized Brain tissue classification of magnetic resonance images: A new approach to the problem of partial volume artifact. *NeuroImage* **2:**133–147.

Carman, G. J., Drury, H. A., and Van Essen, D. C. 1995. Computational Methods for reconstructing and unfolding the cerebral cortex. *Cerebral Cortex.*

Collins, D. L., Neelin, P., Peters, T. M., and Evans, A. C. 1994. Data in Standardized Talairach Space. *J. Comput. Assist. Tomogr.* **18**(2): 292–205.

Culham, J. C., Brandt, S. A., Cavanagh, P., Kanwisher, N. G., Dale, A. M., and Tootell, R. B. H. 1998. Cortical fMRI activation produced by attentive tracking of moving targets. *J. Neurophysiol.*, in press.

Dale, A. M., Fischl, B., and Sereno, M. I. 1998. Cortical Surface-Based Analysis I: Segmentation and Surface Reconstruction. *NeuroImage,* in Press.

Dale, A. M., and Sereno, M. I. 1993. Improved localization of cortical activity by combining EEG and MEG with MRI cortical surface reconstruction: A linear approach. *J. Cogn. Neurosci.* **5**(2):162–176.

Davatzikos, C. 1997. Spatial Transformation and Registration of Brain Images Using Elastically Deformable Models. *Comput. Vision Image Understand.* **66**(2):207–222.

Davatzikos, C., and Bryan, R. N. 1996. Using a Deformable Surface Model to Obtain a Shape Representation of the Cortex. *IEEE Trans. Med. Imag.* **15:**785–795.

DeYoe, E. A., Carman, G. J., Bandettini, P., Glickman, S., Wieser, J., Cox, R., Miller, D., and Neitz, J. 1996. Mapping striate and extrastriate visual areas in human cerebral cortex. *Proc. Natl. Acad. Sci. USA* **93**(6):2382–2386.

Dijkstra, E. W. 1959. A note on two problems in connexion with graphs. *Numerische Mathematik* **1:**269–271.

do Carmo, M. 1976. *Differential Geometry of Curves and Surfaces.* Prentice-Hall, Englewood Cliffs, NJ.

Drury, H. A., Van Essen, D. C., Anderson, C. H., Lee, C. W., Coogan, T. A., and Lewis, J. W. 1996. Computerized Mappings of the Cerebral Cortex: A Multiresolution Flattening Method and a Surface-Based Coordinate System. *J. Cogn. Neurosci.* **8**(1):1–28.

Drury, H. A., Van Essen, D. C., Joshi, S. C., and Miller, M. I. 1996. Analysis and comparison of areal partitioning schemes using two-dimensional fluid deformations. *NeuroImage* **3**(S130).

Drury, H. A., Van Essen, D. C., Snyder, A. Z., Shulman, G. L., Akbudak, E., Ollinger, J. M., Conturo, T. E., Raichle, M., and Corbetta, M. 1997. Warping fMRI activation patterns onto the visible man atlas using fluid deformations of cortical flat maps. *NeuroImage* **5**(S421).

Engel, S. A., Glover, G. H., and Wandell, B. A. 1997. Retinotopic Organization In Human Visual Cortex and the Spatial Precision Of Functional MRI. *Cerebral Cortex* **7**(2):181–192.

Felleman, D., and Van Essen, D. C. 1991. Distributed hierarchical processing in primate cerebral cortex. *Cerebral Cortex* **1:**1–47.

Fischl, B., Dale, A. M., Sereno, M. I., Tootell, R. B. H., and Rosen, B. R. 1998. A coordinate system for the cortical surface. *NeuroImage* **7**(4):S740.

Gauss, K. F. 1828. Disquisitiones generales circa superficies curvas. *Comm. Soc. Gottingen* **Bd 6:**1823–1827.

Hadjikhani, N. K., Liu, A. K., Dale, A. M., Cavanagh, P., and Tootell, R. B. H. 1998. Retinotopy and color sensitivity in human visual cortical area V8. *Nature Neurosci.* **1:**235–241.

Halgren, E., Dale, A. M., Buckner, R. L., Marinkovic, K., Destrieux, C., Fischl, B., and Rosen, B. R. 1998. Cortical location of implicit repetition effects in a size-judgment task to visually-presented words. *NeuroImage,* submitted.

Halgren, E., Dale, A. M., Sereno, M. I., Tootell, R. B. H., Marinkovic, K., and Rosen, B. R. 1998. Location of human face-selective cortex with respect to retinotopic areas. *Hum. Brain Map.*, submitted.

Kaas, J. H., and Krubitzer, L. A. 1991. The organization of extrastriate visual cortex. In *Neuroanatomy of Visual Pathways and their Retinotopic Organization* (B. Dreher and S. R. Robinson, Eds.), Vol. **3,** pp. 302–359. Macmillan, London.

Liu, A. K., Belliveau, J. W., and Dale, A. M. 1998a. Spatiotemporal imaging of human brain activity using fMRI constrained MEG data: Monte Carlo simulations. *Proc. Natl. Acad. Sci. USA* **95:**8945–8950.

Liu, A. K., Dale, A. M., Ahlfors, S., Aronen, H., Huotilainen, M., Ilmoniemi, R., Korvenoja, A., Simpson, G., Tootell, R. B. H., Virtanen, J., and Belliveau, J. W. 1998b. *Spatiotemporal Imaging of Motion Selective Areas in Human Cortex Using Combined fMRI*

and MEG. Seventh Annual Meeting of the International Society for Magnetic Resonance in Medicine, Sydney, Australia. ISMRM, Berkeley, CA.

Liu, A. K., Dale, A. M., Sereno, M. I., Rosen, B. R., and Belliveau, J. W. 1996. *fMRI-Constrained Linear Estimation of Cortical Activity from MEG and EEG Measurements: A Model Study*. Tenth International Conference on Biomagnetism, Santa Fe, NM. Springer Verlag.

MacDonald, D. 1998. *A Method for Identifying Geometrically Simple Surfaces from Three Dimensional Images*. Montreal Neurological Institute, McGill University, Montreal.

Moore, C. I. 1998. Some principles of somatosensory cortical organization in rats and humans. *Brain Cogn. Sci.* MIT, Boston.

Moore, C. I., Gehi, A., Corkin, S., Rosen, B. R., Stern, C., and Dale, A. 1997. *Basic and Fine Somatotopy in Human SI*. The Cognitive Neuroscience Society, San Francisco, CA.

Moore, C. I., Stern, C. E., Corkin, S., Gray, A., Thelusma, F., Rosen, B. R., and Dale, A. M. 1998. Segregation of Multiple Somatosensory Maps within the Human Postcentral Gyrus Using fMRI. *NeuroImage* **7**(4).

Morel, A., and Kaas, J. J. 1992. Subdivisions and connections of auditory cortex in owl monkeys. *J. Comp. Neurol.* **318:**27–63.

Mortenson, M. E. 1997. *Geometric Modeling*. Wiley, New York.

Press, W. H., Teukolsky, S. A., Vetterling, W. T., and Flannery, B. P. 1994. *Numerical Recipes in C*. Cambridge Univ. Press, Cambridge.

Reppas, J. B., Niyogi, S., Dale, A. M., Sereno, M. I., and Tootell, R. B. H. 1997. Representation of motion boundaries in retinotopic human visual cortical areas. *Nature* **388:**175–179.

Schwartz, E. L. 1977. Spatial mapping in the primate sensory projection: Analytic structure and relevance to perception. *Biol. Cybernet.* **25:**181–194.

Schwartz, E. L. 1980. Computational anatomy and functional architecture of striate cortex: A spatial mapping approach to perceptual coding. *Vision Res.* **20:**645–669.

Schwartz, E. L., and Merker, B. 1986. Computer-Aided Neuroanatomy: Differential Geometry of Cortical Surfaces and an Optimal Flattening Algorithm. *IEEE Comp. Graph. Appl.* **6:**36–44.

Schwartz, E. L., Shaw, A., and Wolfson, E. 1989. A numerical solution to the generalized mapmaker's problem: Flattening nonconvex polyhedral surfaces. *IEEE Transactions on Pattern Analysis and Machine Intelligence* **11:**1005–1008.

Sereno, M. I., and Allman, J. M. 1991. Cortical visual areas in mammals. *The Neural Basis of Visual Function* (A. G. Leventhal, Ed.), pp. 160–172. Macmillan, London.

Sereno, M. I., Dale, A. M., Liu, A., and Tootell, R. B. H. 1996. A Surface-based Coordinate System for a Canonical Cortex. *NeuroImage*.

Sereno, M. I., Dale, A. M., Reppas, J. B., Kwong, K. K., Belliveau, J. W., Brady, T. J., Rosen, B. R., and Tootell, R. B. H. 1995. Borders of multiple visual areas in humans revealed by functional magnetic resonance imaging. *Science* **268**(May 12):889–893.

Stepniewska, I., Preuss, T. M., and Kaas, J. H. 1993. Architectonics, somatotopic organization, and ipsilateral cortical connections of the primary motor area (M1) in owl monkeys. *J. Comp. Neurol.* **330:**238–271.

Székely, G., Kelemen, A., Brechbühler, C., and Gerig, G. 1995. *Segmentation of 3D Objects from MRI Volume Data Using Constrained Elastic Deformations of Flexible Fourier Surface Models*. First International Conference on Computer Vision, Virtual Reality and Robotics in Medicine, CVRMed'95, Nice, France.

Talairach, J., Szikla, G., Tournoux, P., Prosalentis, A., Bordas-Ferrier, M., Covello, L., Iacob, M., and Mempel, E. 1967. *Atlas d'Anatomie Stereotaxique du Telencephale*. Masson, Paris.

Talairach, J., and Tournoux, P. 1988. *Co-Planar Stereotaxic Atlas of the Human Brain*. Thieme Medical Publishers, NY.

Talavage. 1998. *Primary Auditory Cortex. HST*. MIT, Boston.

Talavage, T., Ledden, P., MI, S., Rosen, B., and Dale, A. 1997a. Multiple phase-encoded tonotopic maps in human auditory cortex. *NeuroImage* **5**(S8).

Talavage, T., Ledden, P., Sereno, M., Benson, R., Melcher, J., Rosen, B., and Dale, A. 1997b. Phase-encoded tonotopic maps in human auditory cortex. *ISMRM* **5:**6.

Talavage, T., Ledden, P., Sereno, M., Benson, R., and Rosen, B. 1996. Preliminary fMRI evidence for tonotopicity in human auditory cortex. *NeuroImage* **3**(S355).

Talavage, T. M. 1998. Functional magnetic resonance imaging of the frequency organization of human auditory cortex. *Health Sci. Technol.* Boston, MIT.

Teo, P. C., Sapiro, G., and Wandell, B. A. 1997. Creating Connected Representations of Cortical Gray Matter for Functional MRI Visualization. *IEEE Trans. Med. Imag.* **16**(6):852–863.

Thompson, P., Schwartz, C., Lin, R. T., Khan, A. A., and Toga, A. W. 1996. Three-dimensional statistical analysis of sulcal variability in the human brain. *J. Neurosci.* **16**(13):4261–4274.

Thompson, P. M., and Toga, A. W. 1996. A surface-based technique for warping 3-dimensional images of the brain. *IEEE Trans. Med. Imag.* **15:**1–16.

Tootell, R. B. H., Dale, A. M., Mendola, J. D., Reppas, J. B., and Sereno, M. I. 1996a. fMRI analysis of human visual cortical area V3A. *NeuroImage* **3:**S358.

Tootell, R. B. H., Hadjikhani, N. K., Vanduffel, W., Liu, A. K., Mendola, J. D., Sereno, M. I., and Dale, A. M. 1998a. Functional analysis of primary visual cortex (V1) in humans. *Proc. Natl. Acad. Sci. USA* **95:**811–817.

Tootell, R. B. H., Mendola, J. D., Hadjikhani, N. K., Ledden, P. J., Liu, A. K., Reppas, J. B., Sereno, M. I., and Dale, A. M. 1997. Functional analysis of V3A and related areas in human visual cortex. *J. Neurosci.* **17:**7060–7078.

Tootell, R. B. H., Mendola, J. D., Hadjikhani, N. K., Liu, A. K., and Dale, A. M. 1998b. The representation of the ipsilateral visual field in human cerebral cortex. *Proc. Natl. Acad. Sci. USA* **95:**818–824.

Tootell, R. B. H., Reppas, J. B., Dale, A. D., Look, R. B., Malach, R., Jiang, H.-J., Brady, T. J., Rosen, B. R., and Belliveau, J. W. 1995a. Visual motion aftereffect in human cortical area MT/V5 revealed by functional magnetic resonance imaging. *Nature* **375:**139–141.

Tootell, R. B. H., Reppas, J. B., Kwong, K. K., Malach, R., Born, R. T., Brady, T. J., Rosen, B. R., and Belliveau, J. W. 1995b. Functional analysis of human MT and related visual cortical areas using magnetic resonance imaging. *J. Neurosci.* **15**(14):3215–3230.

Tootell, R. H. B., Dale, A. M., Sereno, M. I., and Malach, R. M. 1996b. New images from human visual cortex. *Trends Neurosci.* **19:**481–489.

Van Essen, D. C., and Drury, H. A. 1997. Structural and Functional Analyses of Human Cerebral Cortex Using a Surface-Based Atlas. *J. Neurosci.* **17**(18):7079–7102.

Van Essen, D. C., Drury, H. A., Joshi, S., and Miller, M. I. 1998. Functional and Structural Mapping of Human Cerebral Cortex: Solutions are in the Surfaces. *Proc. Natl. Acad. Sci. USA*.

Wells, W., Grimson, W., Kikinis, R., and Jolesz, F. 1996. Adaptive Segmentation of MRI Data. *IEEE Trans. Med. Imag.* **15**(4):429–442.

Wells, W., Kikinis, R., and Jolesz, F. A. 1994. *Statistical Intensity Correction and Segmentation of Magnetic Resonance Image Data*. Proceedings of the Third Conference on Visualization in Biomedical Computing VBC'94.

Wolfson, E., and Schwartz, E. L. 1989. Computing minimal distances on polyhedral surfaces. *IEEE Trans. Pattern Anal. Machine Intel.* **11:**1001–1005.

Zilles, K., Armstrong, E., Schleicher, A., and Kretschmann, H.-J. 1988. The human pattern of gyrification in the cerebral cortex. *Anat. Embryol.* **179:**173–179.